Journal of Hazardous Materials 211–212 (2012) 68–76

Contents lists available at SciVerse ScienceDirect

Journal of Hazardous Materials

journal homepage: www.elsevier.com/locate/jhazmat

TiO_2/palygorskite composite nanocrystalline films prepared by surfactant templating route: Synergistic effect to the photocatalytic degradation of an azo-dye in water

E. Stathatos[a,*], D. Papoulis[b], C.A. Aggelopoulos[a,c], D. Panagiotaras[d], A. Nikolopoulou[b]

[a] Electrical Engineering Department, Technological-Educational Institute of Patras, GR-26334 Patras, Greece
[b] Department of Geology, University of Patras, GR-26504 Patras, Greece
[c] Foundation for Research and Technology Hellas-Institute of Chemical Engineering and High Temperature Chemical Processes (FORTH/ICE-HT), P.O. Box 1414, GR-26504 Patras, Greece
[d] Mechanical Engineering Department, Technological-Educational Institute of Patras, GR-26334 Patras, Greece

ARTICLE INFO

Article history:
Received 31 May 2011
Received in revised form 28 October 2011
Accepted 16 November 2011
Available online 25 November 2011

Keywords:
Titanium dioxide
Nanocrystalline
Clay mineral
Palygorskite
Photocatalysis
Sol–gel method

ABSTRACT

Microfibrous palygorskite clay mineral and nanocrystalline TiO_2 are incorporating in the preparation of nanocomposite films on glass substrates via sol–gel route at 500 °C. The synthesis involves a simple chemical method employing nonionic surfactant molecule as pore directing agent along with the acetic acid-based sol–gel route without direct addition of water molecules. Drying and thermal treatment of composite films lead to the elimination of organic material while ensure the formation of TiO_2 nanoparticles homogeneously distributed on the surface of the palygorskite microfibers. TiO_2 nanocomposite films without cracks consisted of small crystallites in size (12–16 nm) and anatase crystal phase was found to cover palygorskite microfibers. The composite films were characterized by microscopy techniques, UV–vis, IR spectroscopy, and porosimetry methods in order to examine their structural properties. Palygorskite/TiO_2 composite films with variable quantities of palygorskite (0–2 w/w ratio) were tested as new photocatalysts in the photo-discoloration of Basic Blue 41 azo-dye in water. These nanocomposite films proved to be very promising photocatalysts and highly effective to dye's discoloration in spite of the small amount of immobilized palygorskite/TiO_2 catalyst onto glass substrates. 3:2 palygorskite/TiO_2 weight ratio was finally the most efficient photocatalyst while reproducible discoloration results of the dye were obtained after three cycles with same catalyst. It was also found that palygorskite showed a positive synergistic effect to the TiO_2 photocatalysis.

1. Introduction

Photodegradation of various organic pollutants by photocatalysis, using wide band gap semiconductors under UV or solar light, has been extensively studied [1–3]. Among them, TiO_2 is a relatively inexpensive semiconductor which exhibits high photocatalytic activity, non-toxicity and stability in aqueous solutions [4,5]. Furthermore, the synthesis of mesoporous nanocrystalline anatase TiO_2 particles, films or membranes has extended their use in environmental remediation [6]. Ultrafine titania powders with high particle surface area have good photocatalytic activity since reactions take place on the surface of the nanocatalyst. On the other hand, powders can easily agglomerate in larger particles and as a consequence adverse phenomena to their photocatalytic activity are observed. However, titania is usually used as mobilized catalyst for its high catalytic surface area and activity [7]. Nevertheless, titania powders cannot easily be recovered from aquatic systems when they are used for water treatment. Highly dispersed TiO_2 particles in suspension are difficult to be handled and removed after their application in water and wastewater treatment. Recently, many research studies have been carried out to immobilize TiO_2 catalyst onto various substrates as thin films and membranes. Despite of their lower catalytic surface area, there is an increase to their utilization because of the extension of the field of applications using substrates of different materials, size and shape [8–10]. The specific surface area, particle morphology and possible aggregation, phase composition and number of –OH surface groups are among the most critical parameters for high photocatalytic activity of the as-prepared films. Another approach to enhance the photocatalytic properties of the catalysts is the promotion of their porous structures.

Several procedures have been applied to the immobilization of TiO_2 with enhanced properties and photocatalytic activity. Glass slides and fibers, membranes, activated carbon and zeolites

* Corresponding author. Tel.: +30 2610 369242; fax: +30 2610 369193.
E-mail address: estathatos@teipat.gr (E. Stathatos).

0304-3894/$ – see front matter © 2011 Elsevier B.V. All rights reserved.
doi:10.1016/j.jhazmat.2011.11.055

are used as supports for titania particles [11–14]. The efficiency of photocatalytic procedure is generally decreased with catalyst immobilization as the illuminated total surface area is lower than the case of pure TiO_2 powder. However, the use of highly porous materials such as clay minerals can be considered as alternative substrates for TiO_2 immobilized particles with promising perspectives [15]. Palygorskite clay mineral of hydrated magnesium aluminum silicate with lamellar structure and high surface area could be considered as suitable material for TiO_2 particles immobilization [16,17]. In the present work thin films of mesoporous nanocrystalline TiO_2 in presence of palygorskite microfibers were prepared using a template technique based on the sol–gel method with surfactant molecules. The enhanced photocatalytic efficiency of titania nanoparticles in combination with palygorskite nanocomposite fibers was examined to the discoloration of azo-dye Basic Blue 41 in aqueous solutions. The synergistic effect between TiO_2 and clay mineral fibers was also examined. In spite of the small amount of immobilized TiO_2 catalyst onto glass substrate, the results were very promising when palygorskite was also present. We have chosen to use an azo-dye as a target molecule because dye wastewater pollution from textile industry is one of the major sources of environmental pollution introducing intense coloring and toxicity to the aquatic system. Azo-dyes are extensively used in textile industry and they are very stable to ultraviolet and solar light irradiation. They are also resistant to biological treatment and after reduction carcinogenic aromatic amines can be formed. Photocatalysis is one of the strategies that can be successfully applied to the oxidation and final removal of azo-dyes to the formation of carbon dioxide as a latter product. Moreover, it is the first time that clay mineral/TiO_2 nanocomposite photocatalyst immobilized on glass substrate is referred to the decomposition of an azo-dye in water.

2. Experimental

2.1. Chemicals and materials

Commercially available Triton X-100 (X100, polyethylene glycol tert-octylphenyl ether), titanium tetraisopropoxide (TTIP), acetic acid (AcOH), Basic Blue 41 (BB-41), and all solvents were purchased from Sigma–Aldrich. Palygorskite-rich samples (PAL) from Ventzia continental basin, Western Macedonia Greece, were size fractionated by gravity sedimentation to obtain fillers of less than 2 μm. Most palygorskite rich clay fraction that also characterized by the absence of other clay minerals was used in composite PAL–TiO_2 film preparation. Double distilled water with resistivity 18.2 MΩ (Millipore) was used in all experiments.

2.2. Sol synthesis

The X100 as a long chain nonionic surfactant molecule was selected as a pore directing agent in sol. Compared to other commonly used toxic and ionic templating agents, X100 is relatively inexpensive, biodegradable, and easily removable [18,19]. Such amphiphilic molecules exhibit the existence of ordered mesophase and the ability to adjust large inorganic clusters in aqueous condition [20,21]. A suitable amount of X100 was homogeneously dissolved in ethanol (EtOH). Before adding alkoxide precursor, AcOH was added into the solution for the esterification reaction with EtOH. Then, titania precursor, TTIP was added at a time under vigorous stirring. The molar ratio of the materials was optimized at X100:EtOH:AcOH:TTIP = 1:69:6:1 in accordance to previous results [20]. Small amount of water is released from the esterification reaction of AcOH with ethanol which is employed to the hydrolysis–condensation of TTIP. It is also accepted [6,20] that alkoxy groups bonded to titanium in TTIP can be replaced by acetate groups, forming Ti–OAc and isopropanol (iPrOH). As a result, Ti–O–Ti inorganic network can be formed from the hydrolysis and condensation reactions as shown in Reactions (1)–(4):

$$\text{Ti–OiPr}^* + \text{AcOH} \rightarrow \text{Ti–OAc} + \text{iPrOH} \quad (1)$$

$$\text{iPrOH} + \text{AcOH} \rightarrow \text{iPrOAc} + \text{H}_2\text{O} \quad (2)$$

$$\text{Ti–OAc} + \text{iPrOH} \rightarrow \text{iPrOAc} + \text{Ti–OH} \quad (3)$$

$$\text{Ti–OiPr} + \text{Ti–OAC} \rightarrow \text{iPrOAc} + \text{Ti–O–Ti} \quad (4)$$

*Ti–OiPr is titanium tetraisopropoxide (TTIP) with one of the four alkoxy groups for reasons of simplicity.

In this case, titanium-bonded acetate ligands can be hydrolyzed and participated in a direct condensation reaction, resulting in Ti–O–Ti condensed bridge. However, the true mechanism is very hard to be distinguished but the final product in both cases is oxygen linkages between titanium atoms. Then, palygorskite powder was mixed with previous solution in various quantities following PAL/TiO_2 weight ratio 0:1, 1:2, 1:1, 3:2, 2:1. After several minutes, the dispersion was ready to be used on glass slides. Films prepared on glass slides for the five PAL/TiO_2 weight ratios will be referred as S0, S1, S2, S3 and S4, respectively.

2.3. Formation of TiO_2 thin films and powders

Borosilicate glass with a size of L75 mm (effective L60) × W25 mm × T1 mm was used as a substrate for fabricating immobilized PAL/TiO_2 thin films. Before coating, the substrate was thoroughly cleaned with detergent and washed with water and acetone. The glasses were finally dried in a stream of nitrogen. A home-made dip-coating apparatus equipped with a speed controller to maintain a withdrawal rate of ~10 cm/min was used to dip in and pull out the substrate from the sol. After coating, the films were dried at room temperature for 1 h, calcined in a multi-segment programmable furnace (PLF 110/30, Protherm) at a ramp rate of 5 °C/min to 500 °C for 15 min, and cooled down naturally. Only one layer of catalyst was formed for all PAL/TiO_2 ratios. In the case that powders of the above mentioned samples were prepared, the solutions were put in a rotary evaporator in order to remove the solvent. Then the viscous sols were heat-treated for 2 h at 500 °C instead of 15 min as in making thin films in order to remove all the organic content. In this case the heating ramp rate was 1 °C/min.

2.4. Materials characterization

Chemical analysis of the clay fraction (<2 μm) of palygorskite rich samples were carried out by instrumental neutron activation analysis (INAA) and inductively coupled plasma mass spectroscopy (ICP-MS) using a four acid (HF, $HClO_4$, HNO_3 and HCl) digestion technique. Instrumentation consists of a Thermo Jarrell-Ash ENVIRO II ICP for INAA and a Perkin Elmer Optima 3000 ICP. SiO_2 was determined using X-ray fluorescence method after $LiBO_2$ fusion. A Bruker D8 Advance diffractometer with CuKα (λ = 1.5406 Å) radiation and Bragg-Brentano geometry was employed for X-ray diffraction (XRD) studies of the palygorskite–TiO_2 catalyst. For porosity measurements, the mercury intrusion curves of all samples were taken with a Quantachrome PoreMaster 60 Mercury Porosimeter while the surface area, porosity, and pore size distribution were derived by curves' differentiation. For the visual morphology and inspection of PAL/TiO_2 film homogeneity, an environmental scanning electron microscope (FESEM, Zeiss SUPRA 35VP) was used. Absorption measurements of BB-41 in water were carried out with a Hitachi U-2900 UV–vis spectrophotometer while diffuse

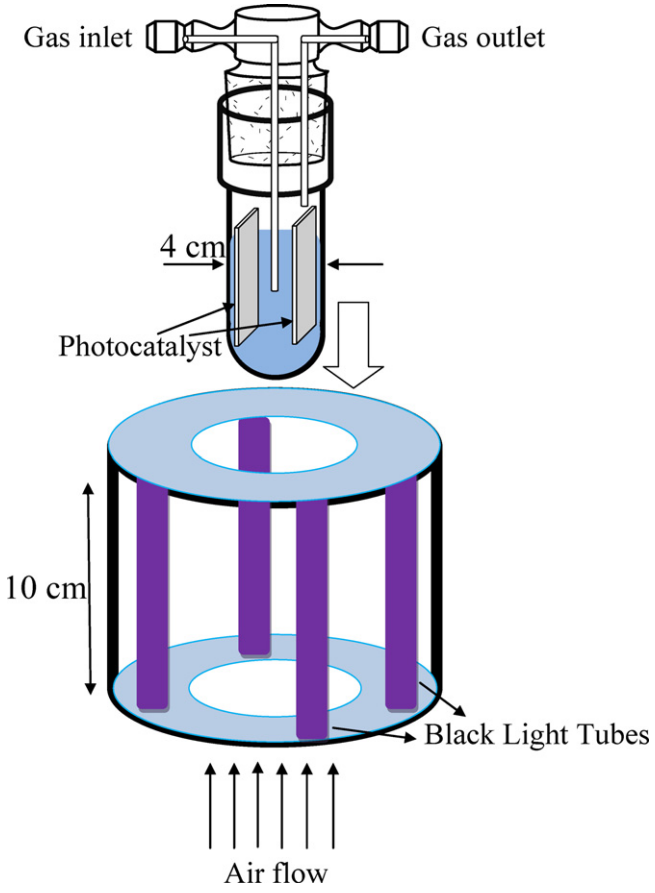

Scheme 1. Schematic representation of the photoreactor used for BB-41 discoloration.

reflectance measurements on photocatalysts were taken in a Varian 1E spectrophotometer equipped with an integration sphere. FT-IR spectra were monitored with a Jasco 4100 spectrophotometer while the films were prepared on silicon wafers avoiding the absorbance of the substrates in the infra red region.

2.5. Photoreactor and photocatalytic activity of PAL–TiO_2 composite films

The cylindrical reactor schematically shown in Scheme 1 was used in all experiments. Air was pumped through the gas inlet using a small pump to ensure continuous oxygen supply to the solution while simultaneously the air agitates it. Four black light fluorescent tubes with nominal power 4 W were placed around the reactor. The whole construction was covered with a cylindrical aluminum reflector. Cooling was achieved by air flow from below the reactor using a ventilator. The catalyst was in the form of four borosilicate glasses, covered on one side with nanocrystalline PAL/TiO_2 film in various w/w proportions specified as samples S0–S4. The total surface area of the films was approximately 60 cm^2 while the photocatalyst mass was 12 mg except the case of pure palygorskite sample stabilized on glass (SP) where the catalyst mass was 16 mg. The intensity of radiation reaching the surface of the films on the side facing lamps was measured with a Solar Light PMA-2100 UV-Photometer and found equal to 0.9 mW/cm^2. The reactor was filled with 80 ml of 2.5×10^{-5} M BB-41 aqueous solution. This dye is strongly adsorbed on TiO_2 modified films. For this reason, we stored the solution in the dark in the presence of the photocatalyst for an hour and all photocatalytic results were obtained after equilibrium. The photo-discoloration process of the dye was examined by monitoring the absorption maximum of the BB-41 solution (at 610 nm) in various irradiation times. Photo-discoloration rate of BB-41 was calculated by the formula: $r = (A_0 - A)/A_0$. Where A_0 is the initial absorbance of BB-41 solution and A is the final absorbance after irradiation with UV light. Discoloration efficiency is determined as $e\% = ((A_0 - A)/A_0) \times 100$. For the repeated use of the photocatalysts, the films were washed with double distilled water and dried at 80 °C while no further treatment was followed for the films. Adsorption of BB-41 on PAL/TiO_2 films was examined under dark and after 1 h presence of the films in dye's aqueous solution.

Table 1
Chemical analyses of palygorskite clay fraction.

Compound	(wt%)
SiO_2	53.17
Al_2O_3	3.96
Fe_2O_3	7.73
MnO	0.032
MgO	12.76
CaO	0.26
Na_2O	0.17
K_2O	0.08
TiO_2	0.18
P_2O_5	0.17
L.O.I.[a]	22.1
Total	100.6

[a] Loss On Ignition (LOI, at 1000 °C) is a measure of the volatile content of a sample. Among other minor constituents, LOI includes structural water from phyllosilicates, absorbed water, CO_2 from carbonate material, and reflects weight changes due to oxidation of organic materials.

3. Results and discussion

3.1. Structural characteristics of PAL/TiO_2 nanocomposites

The chemical analysis of the clay fraction of the palygorskite rich sample is presented in Table 1. As it can be seen, most of the material is consisted of SiO_2 (53.17 wt%) followed by MgO (12.76 wt%) and Fe_2O_3 (7.73 wt%). Aluminum and titanium oxides can be also found in lower contents. Composite palygorskite–TiO_2 films were prepared on borosilicate glass substrates for different PAL/TiO_2 weight proportions as described in Section 2. Samples, abbreviated as S1, S2, S3 and S4 represent the different proportions of palygorskite in TiO_2 sol while S0 is referred to the pure TiO_2 films. Moreover, for pure palygorskite powder immobilized on borosilicate glass substrates we used the same ingredients for the starting solution as in the case of previous samples with only exception the substitution of titanium tetraisopropoxide (TTIP) with aluminum butoxide in order to achieve good adhesion of PAL on glass in presence of an insulator such as alumina (abbreviated as SP). The XRD patterns of all films are presented in Fig. 1. Strong reflection at $2\theta = 8°$ (Fig. 1) is corresponded to palygorskite proving the enhanced crystallinity of the clay mineral (SP). The peaks at $2\theta = 13.7°$, 16.3°, 19.8°, 20.7° represent the Si–O–Si crystalline layer in the clay. Titania pure nanocrystalline film (S0) is also presented in Fig. 1 where a reflection (1 0 1) of anatase form at $2\theta = 25.1°$ is observed. The two basic reflections at $2\theta = 8°$ and $2\theta = 25.1°$ for PAL and TiO_2 are maintained to the rest of samples S1–S4 with different intensity ratio because of the variable proportion between them. The grain size for both PAL and TiO_2 has been calculated from XRD patterns using Scherrer's equation: $D = 0.9\lambda/(s \cos\theta)$, where λ is the wavelength of the X-ray and s is the full width (radians) at half maximum (FWHM) of the signal. The crystallite size for TiO_2 is calculated 14.5, 17.1, 15, 16.7 nm for samples S0, S1, S2, S3, and S4, respectively. All the peaks indicated that the crystal phase of the materials containing titania was anatase and the relatively small width of peaks indicated that the size of the nanocrystallites was less than 17 nm. The

Table 2
Structural characteristics of PAL/TiO_2 powder.

Sample	Total pore volume, V_p (cm^3/g)	Specific surface area, S (m^2/g)	Total porosity, φ	Mean pore diameter, D_{por} (μm)
S0	0.45	44.5	0.539	0.005 (102[a])
SP	3.14	123.1	0.858	18.0
S1	0.77	65.9	0.635	30.1
S2	0.92	82.2	0.662	36.0
S3	1.00	100.0	0.675	26.5
S4	1.21	95.1	0.705	24.7

[a] Concerns the macroporosity between titania aggregates.

palygorskite particle size was also calculated to be from 23 to 35 nm for all samples. It should be noted that it is evident from the XRD patterns that the calcination at 500 °C for 15 min did not cause any phase transformation or destruction of palygorskite. Because of the difficulty in direct characterization of the porosity of immobilized PAL/TiO_2 thin films, the characterizations were carried out on the corresponding particles. Even though the properties of TiO_2 particles obtained from original solutions do not represent well those of films immobilized onto glass substrate, they are useful to quick investigate and compare the effect of sol conditions on the final properties of material. Moreover, the PAL/TiO_2 particles can be used as mobilized catalyst in suspension. The structural characteristics of PAL/TiO_2 particles are shown in Table 2.

As the samples SP and S1, S2, S3, S4 are pure palygorskite or mixtures of palygorskite and titania particles their pore sizes are expected to have a broad range of length scales. To that scope, Hg porosimetry measurements were performed, instead of BET measurements that are, usually, used for the characterization of titania films. Hg porosimetry measurements are performed in order to obtain information for pore sizes larger than 0.5 μm, which are not attainable by gas sorption. The mercury intrusion curves of samples S0, S1, S2, S3, S4 and SP were measured and the pore size distributions were derived by their differentiation (Fig. 2). For sample S0 (Fig. 2b), two types of porosity can be observed. In the porosity formed between titania nanoparticles (microporosity), the mean pore size is expected to be of the same order of magnitude with the mean diameter of nanoparticles (~5 nm). The sharp peak located at 100 μm is believed that it corresponds to the porosity formed between aggregates of titania nanoparticles (macroporosity) and is indicative of the density and homogeneity of this sample. This porosity is, also, apparent in SEM images shown in Fig. 3. The specific surface area S, the total pore volume V_p, the mean pore diameter D_{por}, and the total porosity φ were calculated for all samples and they are presented in Table 2. From data presented for all samples is obvious that palygorskite material is highly porous (85.8%). However, from Fig. 2 is obvious that there is no narrow distribution of palygorskite nanofibers pore size which is also maintained in the case that TiO_2 nanoparticles are used to form a composite material. Nevertheless, TiO_2 particles are also porous (53.9%) while porosity of the composite PAL/TiO_2 material takes values among those referred for palygorskite and TiO_2 as it is also expected. Moreover, high values for the specific surface area of all samples are measured (Table 2). Between samples of PAL/TiO_2 composite material, S3 showed the highest value for particle surface area equal to 100 m^2/g.

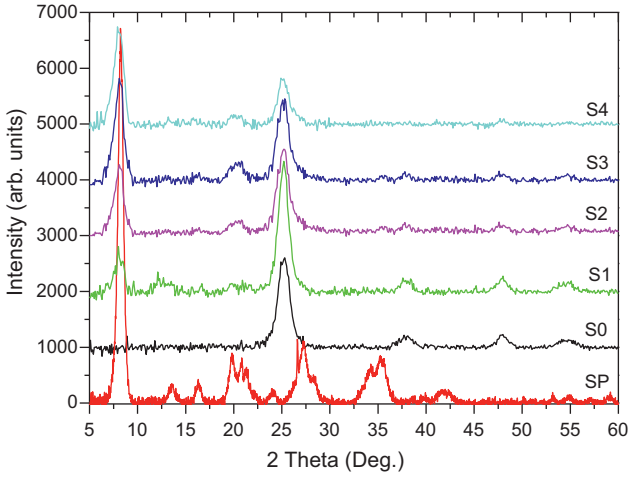

Fig. 1. XRD patterns of PAL–TiO_2 nanocrystalline films.

Palygorskite samples are consisted of fibers in planar structures as it can be seen in Fig. 3a and b. The average diameter of the fibers, as they were observed before modification, is 40 nm while the length is between 500 and 2000 nm (Fig. 3b). After modification, TiO_2 nanoparticles uniform in size overlay palygorskite fibers. Besides, titania nanoparticles help to the stabilization of the composite material on the borosilicate glass substrate after calcination by forming stable Ti–O–Si bonds [22]. In Fig. 3c and d palygorskite microfibers seem to be completely covered with uniform layers of TiO_2 with also uniform particle distribution. The thickness of TiO_2 film without palygorskite fibers is around 180–200 nm according to a cross sectional SEM image. The homogeneity of titania particles' size and film can be seen in Fig. 3e. The TiO_2 crystal grains have a spherical shape while they have an average size ranging from 13 to 16 nm. TiO_2 particles were also found to form aggregates on mineral clay but these were of uniform small size as it was also proved by porosimetry data. The image of the surface of a PAL/TiO_2 film (S3) is also shown in Fig. 3f. The dispersion of palygorskite in TiO_2 films is then obvious but it is firmly agglutinated. No cracks or peeling off traces around palygorskite boundaries were observed. The film is permanently attached on the glass substrate with good adherence while palygorskite cannot be rived from the composite material. Before photocatalytic experiments the films of composite TiO_2 and palygorskite material were rinsed thoroughly with distilled water under pressure. Although powder of palygorskite mineral was used in starting solution which was finally turbid, the resulting film was firmly attached on glass substrates because of TiO_2 (cf. Fig. 3f). The evidences of SEM images for the nanocomposite material may help us to schematic represent the film fabrication on glass substrates (Scheme 2). It is assumed that the organophilic interphase, assured by X100 surfactant coating, acts like a templating medium which provides titanium dioxide nanoparticles with relatively monodispersed particle sizes on the surface. The initially amorphous TiO_2 phase was crystallized after calcination at 500 °C for 15 min in air while X100 was burned out. In agreement with SEM images, the complete coverage of palygorskite surface by metal oxide nanoparticles is achieved most probably when TiO_2 is grafted to the silicate via –Si–O–Ti– bridges contributing to the stability of the nanocomposite material. Thus, silanol groups (Si–OH) of clay mineral can react with titanium alkoxide giving –Si–O–Ti– bridges, which help anchoring titania nanoparticles on palygorskite surface.

The UV–vis diffuse reflectance spectra of pure titania and palygorskite films in comparison with composite PAL/TiO_2 films are presented in Fig. 4. Obviously in the case of sample S4 increasing the quantity of palygorskite in the nanocomposite film there is a short

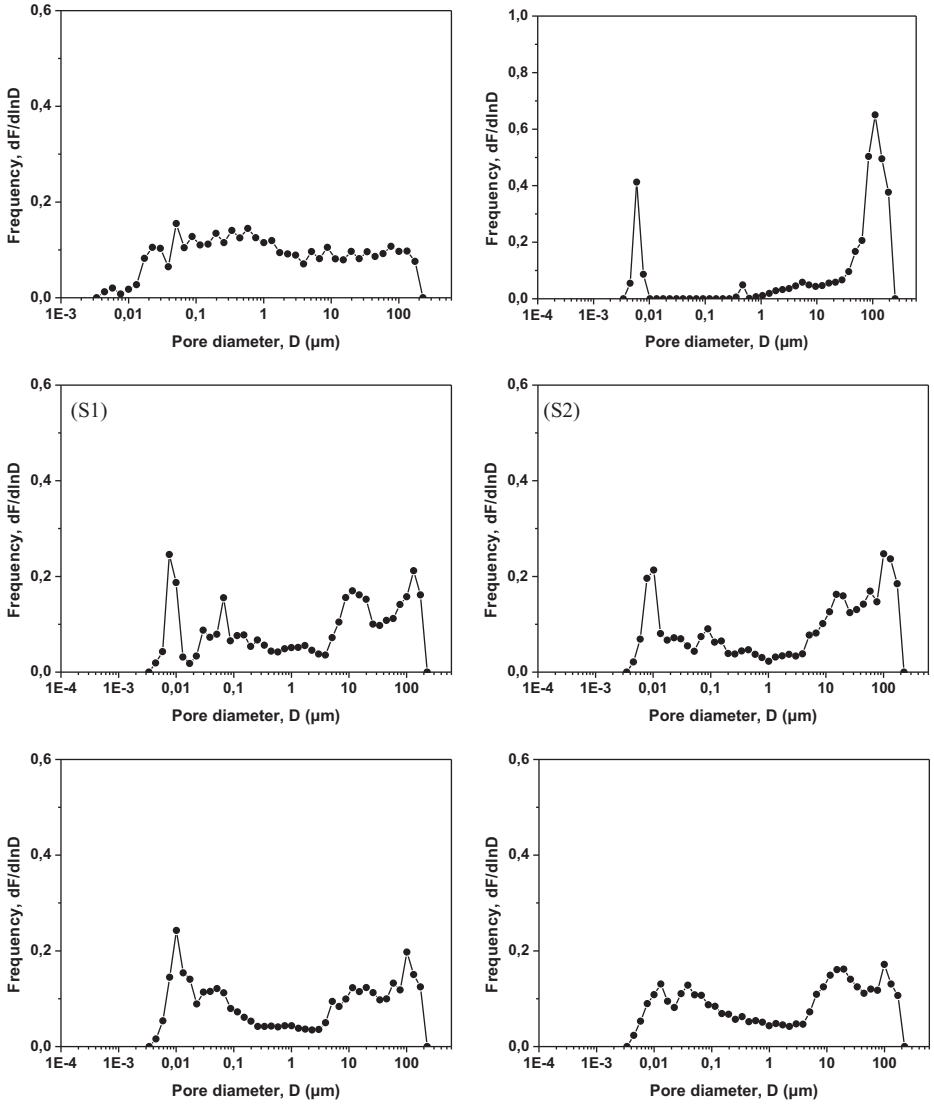

Fig. 2. Pore size distribution for composite PAL–TiO_2 material.

shift in the absorbance at longer wavelengths because of different slope to the absorbance onset. This is caused to pure clay mineral which is colored light brown confirmed by the long tail in the visible (SP). The extent of the absorption of composite PAL/TiO_2 films at longer wavelengths compared to pure TiO_2 films could be somehow affected to the photocatalytic properties of the catalyst examined to the next section. Furthermore, from IR absorbance of palygorskite modified films as presented in Fig. 5b, there is a new peak appeared in 1015 cm^{-1} which is ascribed to Si–O–Ti stretching mode [23] that it does not exist in pure palygorskite clay mineral (Fig. 5a). The basic palygorskite peak located at 1108 cm^{-1} appears as a shoulder of the more intense peak at 1015 cm^{-1}. The existence of this peak could be an explanation for the photocatalytic activity of composite PAL/TiO_2 films [24,25]. Peak located in the area of 400–650 cm^{-1} correspond to the vibration of Ti–O and Ti–O–O bonds. It is noted that the examination of the films in IR was made on silicon wafer. It is also clear from data of Fig. 5b that there are no IR absorption peaks corresponding to impurities like organic residues, –CH and $–CH_2$ in 1400–2900 cm^{-1} and C–O–C in 1000–1500 cm^{-1}. The intense peak observed in 1108 cm^{-1} in pure palygorskite sample (Fig. 5a) is ascribed to Si–O stretching mode. A wide peak centered at 3382 cm^{-1} was also observed at PAL/TiO_2 films and it is ascribed to stretching vibrations of hydroxyl groups which are absolutely necessary for the photocatalytic processes. A band at 1644 cm^{-1} was also found that is ascribed to bending mode of coordinated adsorbed water [26].

3.2. Photocatalytic activity of modified palygorskite PAL/TiO_2 films

Photocatalytic experiments were undertaken on Basic Blue 41 to evaluate PAL–TiO_2 composite catalyst in films as shown in Fig. 6. Various ratios of palygorskite–TiO_2 showed differences to the photocatalytic activities of the films. The rate of discolorization was monitored with respect to the change in intensity with time of the absorption peak at 610 nm. The absorption peak of the dye diminished with time and disappeared during the reaction indicating that it had been discolorized and as a consequence decomposition is caused to the molecule. The discoloration of BB-41 is mainly due to the heterocyclic ring of the molecule which is more vulnerable to splitting [27]. Furthermore, the initial pH value of the BB-41 at $t = 0$ min was found to be 6.5 while no perceivable changes were monitored during photocatalytic experiments. Besides, the UV illumination was started after one hour of the photocatalyst presence in dye's sol in order to be in equilibrium before illumination. The results also showed that there was no direct photolysis of

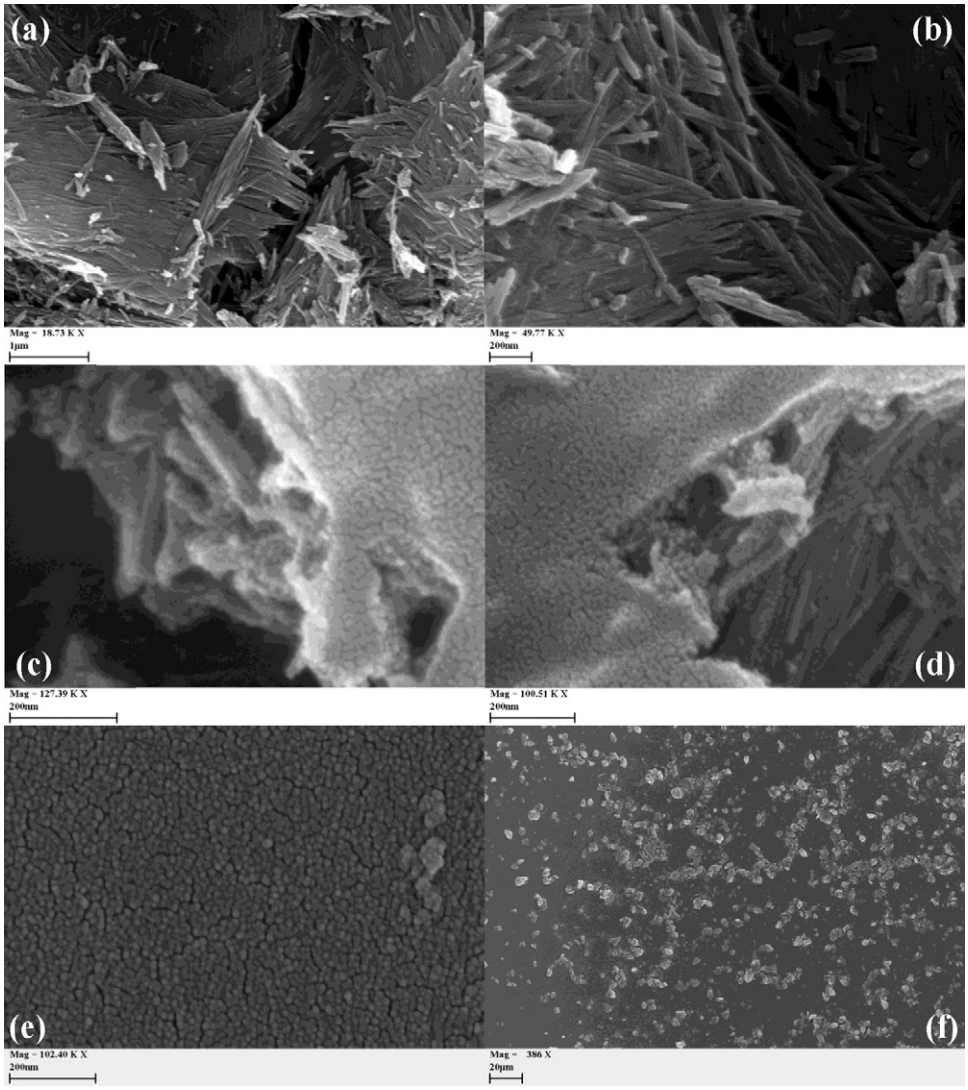

Fig. 3. FE-SEM images: of palygorskite fibers (a) in low and (b) high magnification. Modification with TiO_2 particles (composite PAL–TiO_2) film (S3) appear in (c) and (d) in high magnification. Titania particles are depicted on image (e) after selective magnification on S3 film. (f) Surface of S3 film.

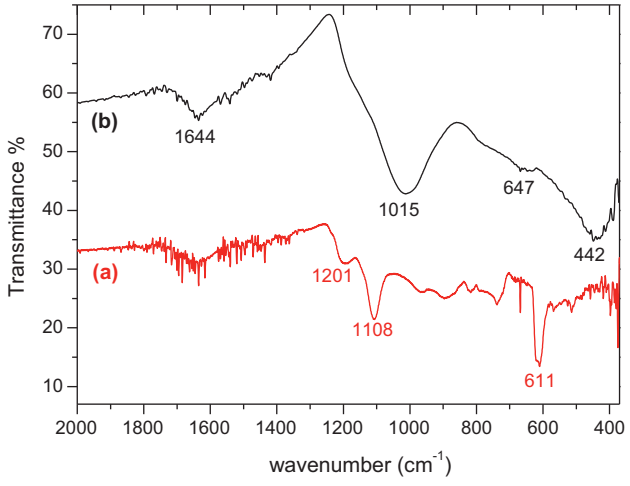

Fig. 5. FTIR spectra of (a) palygorskite clay mineral and (b) PAL–TiO_2 nanocomposite film (S3) on silicon wafer.

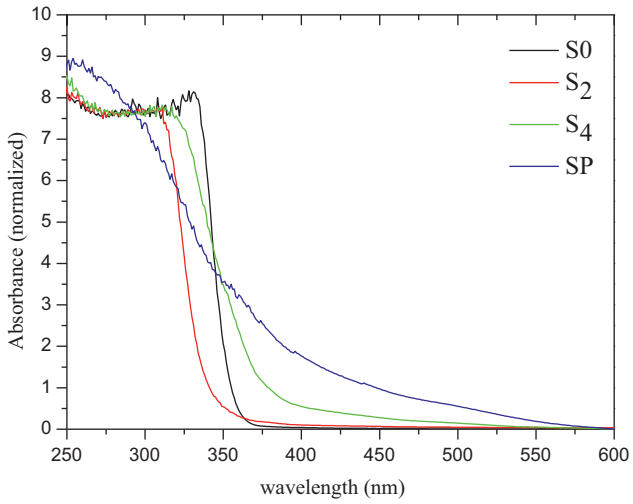

Fig. 4. UV–vis diffuse reflectance spectra of nanocomposite films.

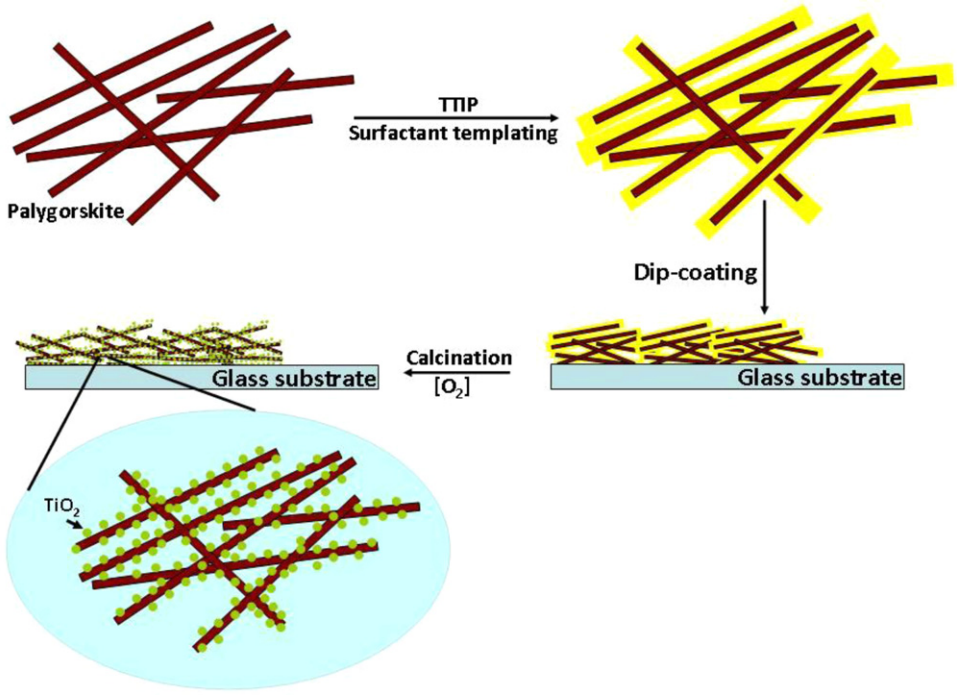

Scheme 2. Procedure of PAL–TiO_2 nanocomposite photocatalyst formation after calcination to promote TiO_2 nanoparticles.

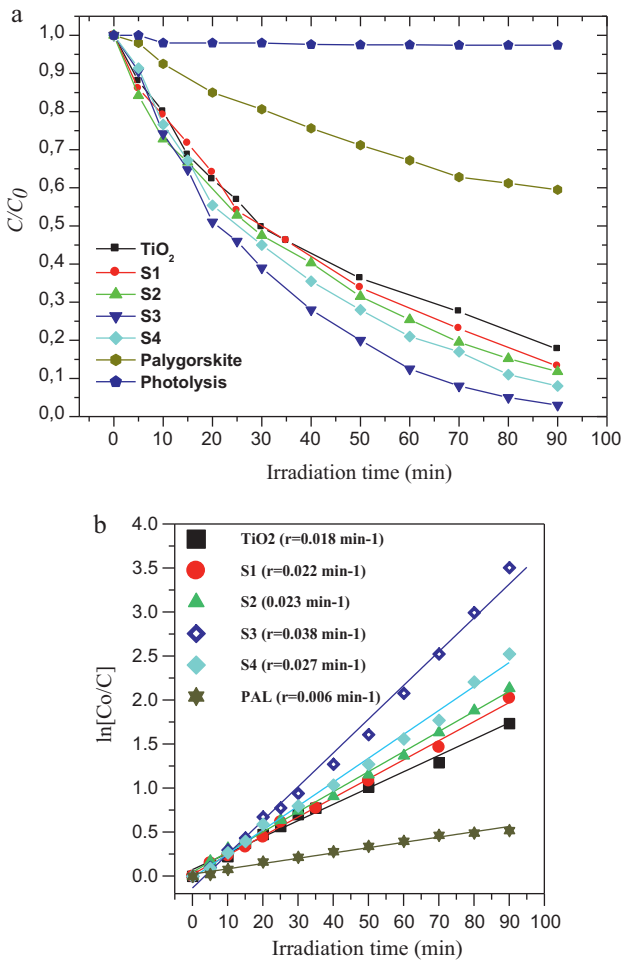

Fig. 6. (a) Photodecoloration of BB-41 by different catalysts and (b) $\ln(C_0/C)$ as a function of irradiation time for PAL–TiO_2 photocatalysts.

BB-41 in the absence of photocatalysts. In the case of S3 a complete discoloration was reached within 90 min of illumination implied the synergistic effect between palygorskite and TiO_2 by preparing highly porous PAL/TiO_2 catalysts. However, the further addition of palygorskite in films (S4) caused a slight decrease to the photocatalytic activity of the films mainly due to a limit of the palygorskite addition for enhanced properties of the composite photocatalyst. Moreover, considering the small amount of TiO_2 catalyst immobilized onto the substrate, the PAL/TiO_2 films were highly efficient to degrade the organic dye. Also from data of Fig. 6a seems that palygorskite has a low photocatalytic response in UV light most probably to the presence of light activated oxides that contains such as Fe_2O_3, TiO_2 while the co-existence of MgO and CaO could help to the better hydroxylation of the surface [28] or to slower charge recombination [29], respectively. As a consequence, the microfibrous nanocomposite material can behave as a photocatalyst acting separately from anatase nanoparticles, showing in this way a synergistic effect. The enhanced performance of S3 compared to the rest of the samples is attributed to the better particle surface area. Discoloration kinetics of BB-41 has been observed to follow first-order kinetics and it is well established that photocatalytic experiments follow Langmuir–Hinshelwood model, where the reaction rate, r, is proportional to the surface coverage, θ, according to the following equation [30]:

$$r = -\frac{dC}{dt} = k_1\vartheta = \frac{k_1 KC}{1+KC} \quad (5)$$

where k_1 is the reaction rate constant, K is the adsorption coefficient of the reactant and C is the reactant concentration. In the case that C is very small, KC factor is negligible in respect to unity and Eq. (5) describes a first-order kinetics. The integration of Eq. (5) yields to Eq. (6):

$$-\ln\left(\frac{C}{C_0}\right) = k_{app}t \quad (6)$$

with limit condition that on $t=0$ we have the initial concentration C_0. k_{app} is the apparent first-order rate constant. Discoloration kinetics of BB-41 in presence of different PAL/TiO_2 proportions is

Table 3
Constant of BB-41 discoloration rate and concentration in equilibrium.

Sample	k_{app} ($\times 10^{-3}$ min^{-1})	C_f ($\times 10^{-5}$ M)
S0	18	0.34
SP	6	1.36
S1	22	0.50
S2	23	0.59
S3	38	0.70
S4	27	0.82

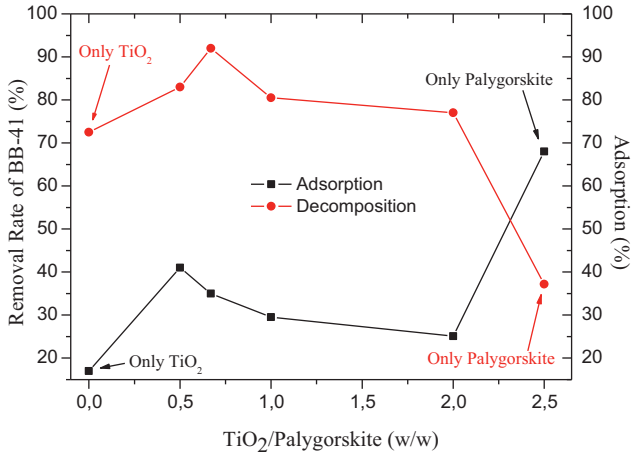

Fig. 7. Correlation between adsorption and photodecoloration rate of BB-41 by PAL–TiO_2 photocatalysts.

presented in Fig. 6b. The maximum value for rate constant was calculated for sample S3 (38×10^{-3} min^{-1}) while the value for pure TiO_2 film was estimated at 18×10^{-3} min^{-1} (Table 3). Furthermore, all the samples PAL/TiO_2 exhibited better performance than pure TiO_2. This is attributed to better structural characteristics of the films compared to pure titania film tabulated at porosity and particle surface area. Besides from data of Table 3 is obvious that the adsorbed quantity of BB-41 is higher in the case that palygorskite/TiO_2 composite material is used. The rate of dye's discoloration clearly depends on adsorption of the dye into the catalyst porous structure (Fig. 7). In particular, maximum photocatalytic efficiency was found at 2:3 TiO_2/palygorskite weight ratio (S3). Furthermore, the catalyst is found to be highly porous mainly to the presence of clay mineral. For this TiO_2/palygorskite weight ratio

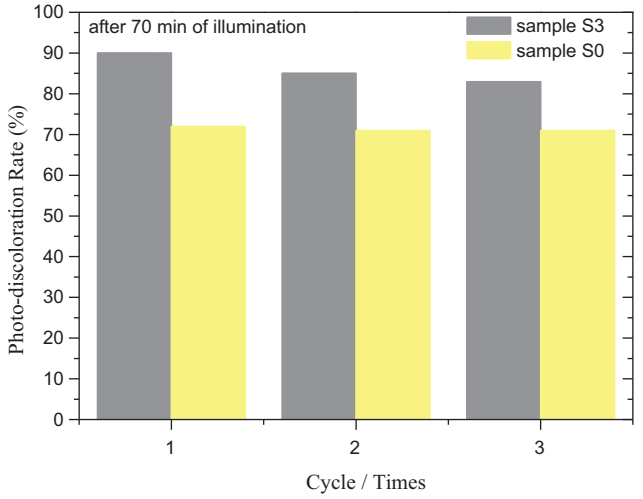

Fig. 8. Reproducibility of BB-41 discoloration within 70 min over S3 photocatalyst for three cycles.

the dye adsorption was very high and very close to the maximum recorded. Finally, it has been found that the same photocatalyst can be used in several photocatalytic cycles without remarkable loss to its efficiency. The discoloration of BB-41 over S3 photocatalyst after three successive circles can be seen in Fig. 8. Films consisted of pure nanocrystalline TiO_2 are also presented for reasons of comparison.

4. Conclusions

Highly porous nanostructured PAL/TiO_2 particles and films were synthesized via sol–gel method composed of ethanol, acetic acid, titanium tetraisopropoxide, palygorskite nanofibers and nonionic surfactant molecules (X100) as templates. Slow hydrolysis reaction and stable incorporation of inorganic network onto surfactant molecules made it possible to control the subsequent porous nanostructure. The PAL–TiO_2 films exhibited enhanced structural properties including crystallinity and active anatase phase while enhanced photocatalytic properties to the discoloration of BB-41 in water were succeeded. The experiments on photocatalytic discoloration of BB-41 indicated the importance of preparing highly porous PAL/TiO_2 films where a synergistic effect between palygorskite microfibers and TiO_2 nanoparticles could be occurred.

Acknowledgements

The authors are very thankful to Prof. Christos Kordulis, Dept. of Chemistry, University of Patras, for the Diffuse Reflectance Spectroscopy measurements, and Dr. Vassilios Dracopoulos, FORTH/ICE-HT, for the FESEM images and XRD diffractograms.

References

[1] M.N. Chong, B. Jin, C.W.K. Chow, C. Saint, Recent developments in photocatalytic water treatment technology: a review, Water Res. 44 (2010) 2997–3027.
[2] H. Choi, S.R. Al-Abed, D.D. Dionysiou, E. Stathatos, P. Lianos, TiO_2-based advanced oxidation nanotechnologies for water purification and reuse, Chapter 8, Sustain. Sci. Eng. 2 (2010) 229–254.
[3] S. Ahmed, M.G. Rasul, W.N. Martens, R. Brown, M.A. Hashib, Heterogeneous photocatalytic degradation of phenols in wastewater: a review on current status and developments, Desalination 261 (2010) 3–18.
[4] V.A. Sakkas, Md. A. Islam, C. Stalikas, T.A. Albanis, Photocatalytic degradation using design of experiments: a review and example of the Congo red degradation, J. Hazard. Mater. 175 (2010) 33–44.
[5] H. Choi, E. Stathatos, D.D. Dionysiou, Photocatalytic TiO_2 films and membranes for the development of efficient wastewater treatment and reuse systems, Desalination 202 (2007) 199–206.
[6] H. Choi, E. Stathatos, D.D. Dionysiou, Sol–gel preparation of mesoporous photocatalytic TiO_2 films and TiO_2/Al_2O_3 composite membranes for environmental applications, Appl. Catal. B: Environ. 63 (2006) 60–67.
[7] M.I. Litter, Heterogeneous photocatalysis: transition metal ions in photocatalytic systems, Appl. Catal. B: Environ. 23 (1999) 89–114.
[8] X.-M. Song, J.-M. Wu, M. Yan, Photocatalytic degradation of selected dyes by titania thin films with various nanostructures, Thin Solid Films 517 (2009) 4341–4347.
[9] M. Bizarro, M.A. Tapia-Rodríguez, M.L. Ojeda, J.C. Alonso, A. Ortiz, Photocatalytic activity enhancement of TiO_2 films by micro and nanostructured surface modification, Appl. Surf. Sci. 255 (2009) 6274–6278.
[10] M. Pelaez, P. Falaras, V. Likodimos, A.G. Kontos, A.A. de la Cruz, K. O'shea, D.D. Dionysiou, Synthesis, structural characterization and evaluation of sol–gel-based NF–TiO_2 films with visible light-photoactivation for the removal of microcystin-LR, Appl. Catal. B: Environ. 99 (2010) 378–387.
[11] X. Wang, Y. Liu, Z. Hu, Y. Chen, W. Liu, G. Zhao, Degradation of methyl orange by composite photocatalysts nano-TiO_2 immobilized on activated carbons of different porosities, J. Hazard. Mater. 169 (2009) 1061–1067.
[12] F. Li, S. Sun, Y. Jiang, M. Xia, M. Sun, B. Xue, Photodegradation of an azo dye using immobilized nanoparticles of TiO_2 supported by natural porous mineral, J. Hazard. Mater. 152 (2008) 1037–1044.
[13] G. Rose, M. Echavia, F. Matzusawa, N. Negishi, Photocatalytic degradation of organophosphate and phosphonoglycine pesticides using TiO_2 immobilized on silica gel, Chemosphere 76 (2009) 595–600.
[14] C.-C. Wang, C.-K. Lee, M.-D. Lyu, L.-C. Juang, Photocatalytic degradation of C.I. Basic Violet 10 using TiO_2 catalysts supported by Y zeolite: an investigation of the effects of operational parameters, Dyes and Pigments 76 (2008) 817–824.
[15] T. An, J. Chen, G. Li, X. Ding, G. Sheng, J. Fu, B. Mai, K.E. O'Shea, Characterization and the photocatalytic activity of TiO_2 immobilized hydrophobic

montmorillonite photocatalysts: degradation of decabromodiphenyl ether (BDE 209), Catal. Today 139 (2008) 69–76.
[16] L. Bouna, B. Rhouta, M. Amjoud, F. Maury, M.-C. Lafont, A. Jada, F. Senocq, L. Daoudi, Synthesis, characterization and photocatalytic activity of TiO_2 supported natural palygorskite microfibers, Appl. Clay Sci. 52 (2011) 301–311.
[17] D. Papoulis, S. Komarneni, A. Nikolopoulou, P. Tsolis-Katagas, D. Panagiotaras, H.G. Kacandes, P. Zhang, S. Yin, T. Sato, H. Katsuki, Palygorskite- and halloysite–TiO_2 nanocomposites: synthesis and photocatalytic activity, Appl. Clay Sci. 50 (2010) 118–124.
[18] Y. Wang, Z.-H. Jiang, F.-J. Yang, Preparation and photocatalytic activity of mesoporous TiO_2 derived from hydrolysis condensation with TX-100 as template, Mater. Sci. Eng. B 128 (2006) 229.
[19] P.K. Mohan, G. Nakhla, E.K. Yanful, Biodegradability of surfactants under aerobic, anoxic, and anaerobic conditions, J. Environ. Eng. 132 (2006) 279.
[20] E. Stathatos, P. Lianos, C. Tsakiroglou, Highly efficient nanocrystalline titania films made from organic/inorganic nanocomposite gels, Microporous Mesoporous Mater. 75 (2004) 255–260.
[21] H. Choi, E. Stathatos, D.D. Dionysiou, Synthesis of nanocrystalline photocatalytic TiO_2 thin films and particles using sol–gel method modified with nonionic surfactants, Thin Solid Films 510 (2006) 107–114.
[22] E. Stathatos, P. Lianos, F. Del Monte, D. Levy, D. Tsiourvas, Formation of TiO_2 nanoparticles in reverse micelles and their deposition as thin films on glass substrates, Langmuir 13 (1997) 4295–4300.
[23] J.-C. Liu, M_x–O_y–Si_z bonding models for silica-supported Ziegler-Natta catalysts, Appl. Organomet. Chem. 13 (1999) 295–302.
[24] M. Bellardita, M. Addamo, A. Di Paola, G. Marcì, L. Palmisano, L. Cassar, M. Borsa, Photocatalytic activity of TiO_2/SiO_2 systems, J. Hazard. Mater. 174 (2010) 707–713.
[25] D.M. Tobaldi, A. Tucci, A. Sever Škapin, L. Esposito, Effects of SiO_2 addition on TiO_2 crystal structure and photocatalytic activity, J. Eur. Ceram. Soc. 30 (2010) 2481–2490.
[26] J. Araña, A. Peña Alonso, J.M. Doña Rodríguez, G. Colón, J.A. Navío, J. Pérez Peña, FTIR study of photocatalytic degradation of 2-propanol in gas phase with different TiO_2 catalysts, Appl. Catal. B: Environ. 89 (2009) 204–213.
[27] I.K. Konstantinou, T.A. Albanis, TiO_2-assisted photocatalytic degradation of azo dyes in aqueous solution: kinetic and mechanistic investigations: a review, Appl. Catal. B: Environ. 49 (2004) 1.
[28] H.S. Jung, J.-K. Lee, M. Nastasi, J.-R. Kim, S.-W. Lee, J.Y. Kim, J.-S. Park, K.S. Hong, H. Shin, Enhancing photocatalytic activity by using TiO_2–MgO core–shell-structured nanoparticles, Appl. Phys. Lett. 88 (2006) 013107.
[29] L. Song, S. Zhang, A simple mechanical mixing method for preparation of visible-light-sensitive NiO–CaO composite photocatalysts with high photocatalytic activity, J. Hazard. Mater. 174 (2010) 563–566.
[30] A.O. Ibhadon, G.M. Greenway, Y. Yue, P. Falaras, D. Tsoukleris, The photocatalytic activity and kinetics of the degradation of an anionic azo-dye in a UV irradiated porous titania foam, Appl. Catal. B: Environ. 84 (2008) 351–355.